Charge-dependent directed flow in Cu+Au collisions at $\sqrt{s_{\rm NN}} = 200$ GeV

Takafumi Niida and Sergei A. Voloshin
Wayne State University

May 31, 2016

Abstract

This note presents the analysis detail of charge-dependent directed flow in Cu+Au collisions at $\sqrt{s_{NN}} = 200$ GeV.

Contents

1 Introduction

At the early stages of non-central heavy-ion collisions, a strong magnetic field perpendicular to the reaction plane is created. In asymmetric Cu+Au collisions, due to the difference in the number of spectators, not only the magnetic field but also a strong electric field (E-field) would be created along the reaction plane and pointing from the Au-nucleus to Cu-nucleus. The lifetime of the E-field would be short, of the order of a fraction of a fm/c [1, 2]. The quarks and antiquarks that have been already produced at this time would experience the Coulomb force, which result in charge separation of directed flow [2]. Thus, the measurement of the charge-dependent directed flow in Cu+Au provides an opportunity to test different quark (charge) scenarios, e.g two-wave quark production by S. Pratt, and shed light on the (anti-)quark production mechanism in heavy-ion collisions in general.

2 Analysis

2.1 Data set and event selection

Data from run12 Cu+Au collisions at $\sqrt{s_{NN}} = 200$ GeV was used in this analysis. The following event selections were required for the minimum bias trigger events (vpd-zdce-tac-protected and vpd-zdc-mb-protected).

- cuAu_production_2012, P15ie
- Trigger ID used: 410008 and 410005
- $|v_z| < 30$ cm
- $|v_r| < 2$ cm from the center (vertex position in transverse plane)
- $|v_z - v_z^{vpd}| < 3$ cm

Then run QA was performed by looking at $\langle$RefMult$\rangle$, $\langle v_x \rangle$, $\langle v_y \rangle$, $\langle v_z \rangle$, $\langle p_T \rangle$, $\langle$DCA$\rangle$ and the number of events. This analysis uses event planes reconstructed by ZDC-SMD, BBC, and EEMC in addition to TPC. Therefore the adc sum of ZDC and BBC for both east and west sides and the average energy of total towers in EEMC were also checked with run numbers. Figure 1 and Figure 2 show those variables as a function of run index. Runs 2.5σ away from their averages were marked as bad runs (red symbols). Total 12 bad runs were removed from this analysis, which are listed below.

- 13139063, 13139064, 13139065, 13139066, 13139067, 13139072, 13139073, 13139074, 13139080, 13143037, 13145005, 13147030

Figure 3 shows RefMult distribution (black line) for selected z-vertex bin, where a "tail" in high RefMult events can be seen. It would be probably due to the pile up events. Figure 4 show the correlation between RefMult and TofMult and the correlation between RefMult and BBC acc sum in east side. Some strange events like low RefMult with high TofMult and low TofMult with high RefMult are seen. Those strange events were removed from this analysis based on the correlation of RefMult and TofMult.

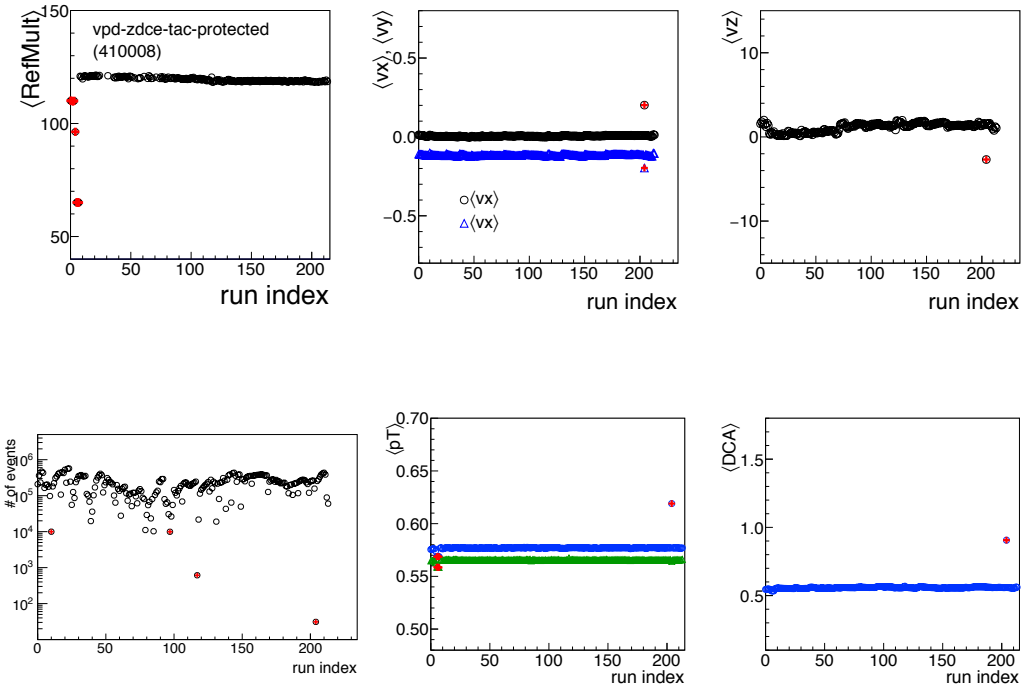

Fig. 1: Run dependence of $\langle \text{RefMult} \rangle$, $\langle v_x \rangle$, $\langle v_y \rangle$, $\langle v_z \rangle$, $\langle p_T \rangle$, $\langle \text{DCA} \rangle$ and the number of events

2.2 Track selection

The basic cuts for track selection are summarized below:

- $0.15 < p_T < 5$ GeV/c
- $|\eta| < 1$
- nHitsFit>=15
- nHistFit/nHitsPoss>=0.52
- gDCA<3 cm

In the reconstruction of the event plane, the p_T range is limited to $0.15 < p_T < 2$ GeV/c.

2.3 Centrality calibration

After selecting good runs and good events, the centrality calibration was performed using Glauber simulation software used at STAR (offline/users/hmasui/Glauber). The data of 5M events was generated for Cu+Au collisions with deformed nuclei. Before doing Glauber+NBD fitting to RefMult distribution, the luminosity dependence of

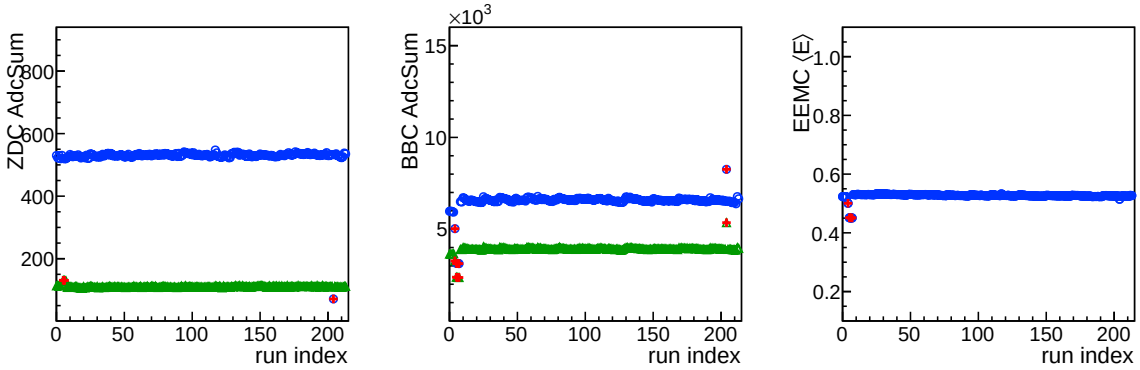

Fig. 2: Run dependence of ZDC adc sum, BBC adc sum, and mean energy of all towers in EEMC, where blue symbols in left two panes show east side of each detector and green symbols show west side.

RefMult was corrected to be independent of the luminosity (ZDC coincidence rate). Then the fitting was performed each v_z bin (5 cm step). The detail can be found in the following material:

`http://www.star.bnl.gov/protected/bulkcorr/taknn/2015/0729_BulkCorr_CuAuUpdate_niida.pdf`

Centrality definition used in this analysis is summarized in Table 1.

2.4 Event plane calibration

2.4.1 Event plane reconstruction

For flow measurements, event planes were reconstructed by ZDC-SMD, BBC, TPC, and EEMC using the following formula:

$$\Psi_n = \frac{1}{n}\tan^{-1}\left(\frac{Q_{n,y}}{Q_{n,x}}\right) \quad (1)$$

$$Q_{n,x} = \sum w_i \cos(n\phi_i)/\sqrt{\sum w_i} \quad (2)$$

$$Q_{n,y} = \sum w_i \sin(n\phi_i)/\sqrt{\sum w_i} \quad (3)$$

where w_i is the weight of particle i (TPC) or segment/tower i (ZDC,BBC,EEMC) and ϕ is an azimuthal angle. In case of TPC, p_T of tracks ($0.15< p_T <2$ GeV/c) was used as the weight. The adc or energy ($E_T < 2$ GeV/c) were used for BBC and EEMC.

The event plane is expected to direct to random direction in event-by-event, but the uncorrected event plane distribution is usually not flat due to imperfect detector acceptance. Therefore the event plane calibration was performed by two steps: re-centering and flattening corrections [3]. The calibration was performed in run-by-run basis, 5% centrality step, 6 cm z-vertex step. Figure 5, 6, 7, 8 show reconstructed event planes of each detector before and after the calibration for 20-20% centrality bin.

Table 1: Centrality definition in Cu+Au collisions, where the values of RefMult is after the correction for luminosity dependence.

Centrality	RefMult
0-5%	>273
5-10%	235
10-15%	201
15-20%	170
20-25%	142
25-30%	118
30-35%	97
35-40%	78
40-45%	62
45-50%	49
50-55%	38
55-60%	29
60-65%	22
65-70%	16
70-75%	12
75-80%	8

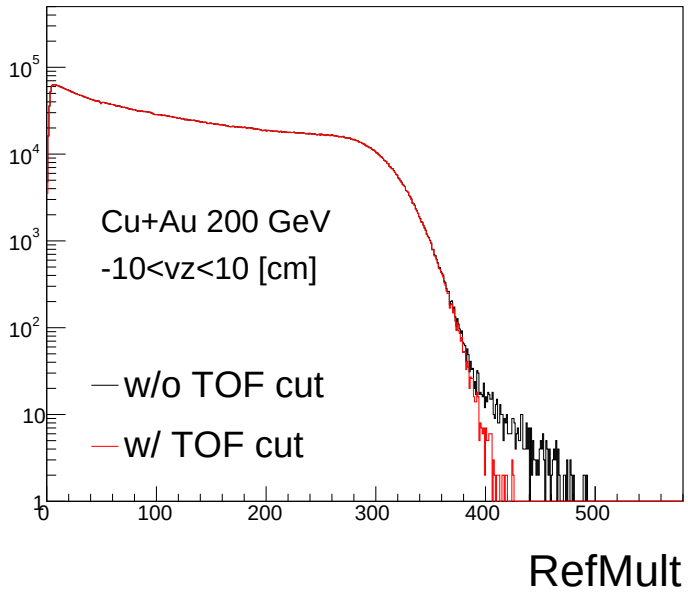

Fig. 3: RefMult distribution in $-5 < v_z < 5$ cm with and without TofMult cut

2.4.2 Event plane QA

After the calibration, the event plane distributions should be flat. As a check, each event plane distribution was fitted with constant function. The obtained χ^2/NDF were plotted in Fig.9, 10, 11, 12. Basically the event planes are well calibrated, but some event class for ZDC and BBC shows larger χ^2/NDF, probably due to worse event plane resolution. Such event planes were not used in this analysis.

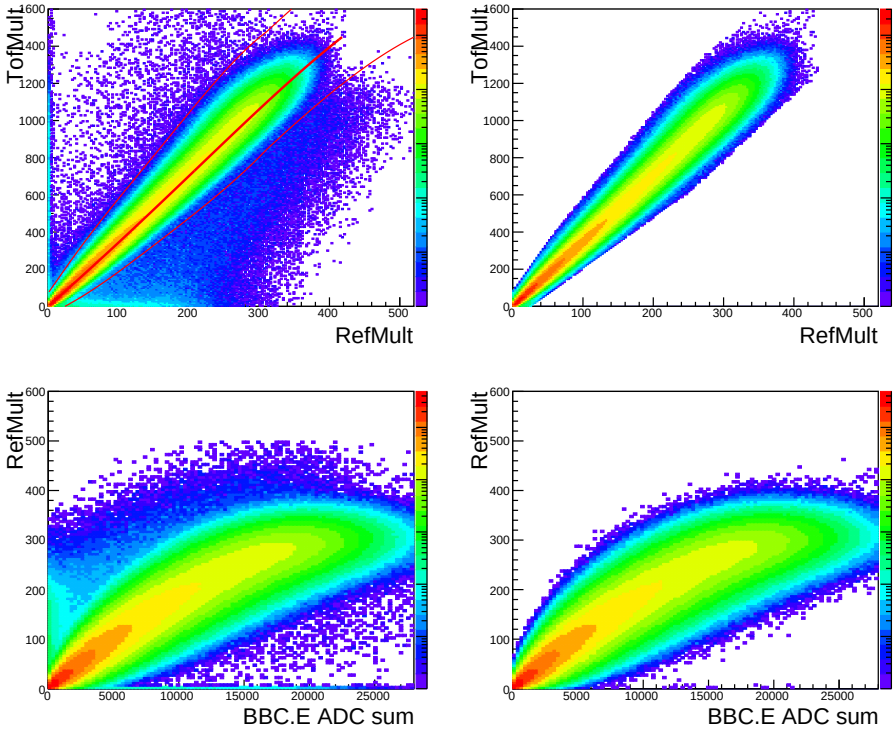

Fig. 4: Correlation between RefMult and TofMult (top two panes) and the correlation between RefMult and BBC acc sum in east side (bottom two panels). Left two panes are plots without TofMult cut and right panels are those with TofMult cut. The TofMult cut is shown as red thin lines in right upper panel.

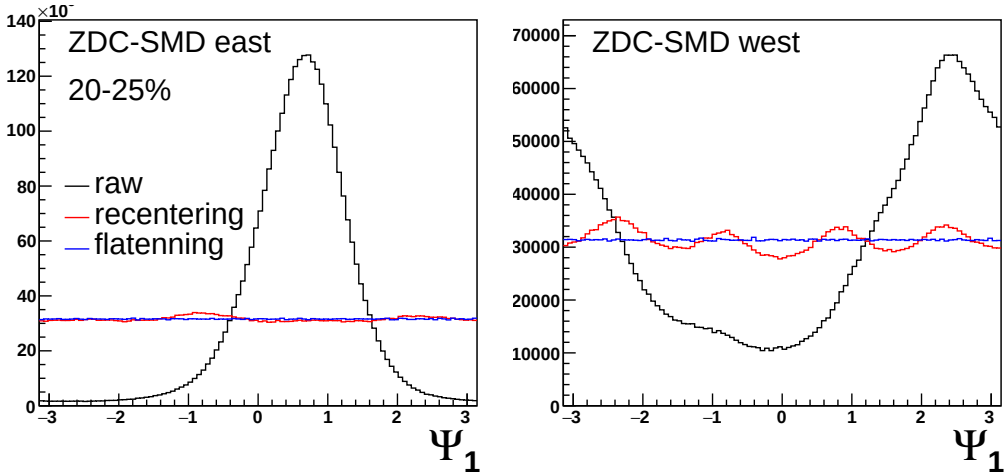

Fig. 5: First-order event plane distributions reconstructed by ZDC-SMD in both east and west sides before and after the calibration in 20-25% centrality.

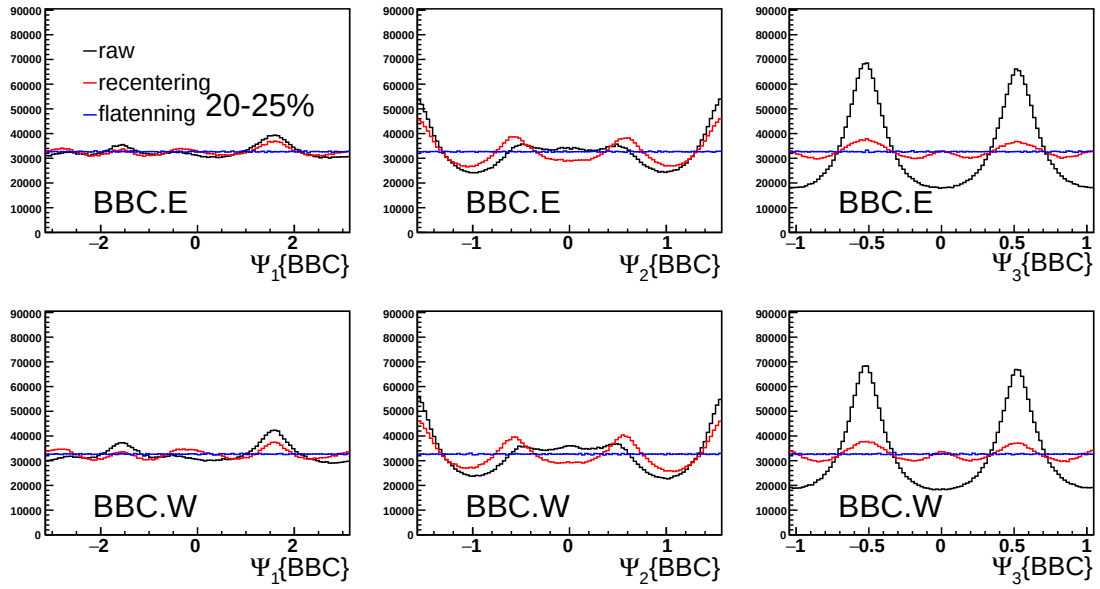

Fig. 6: First-, second-, and third-order event plane distributions reconstructed by BBC in both east and west sides before and after the calibration in 20-25% centrality.

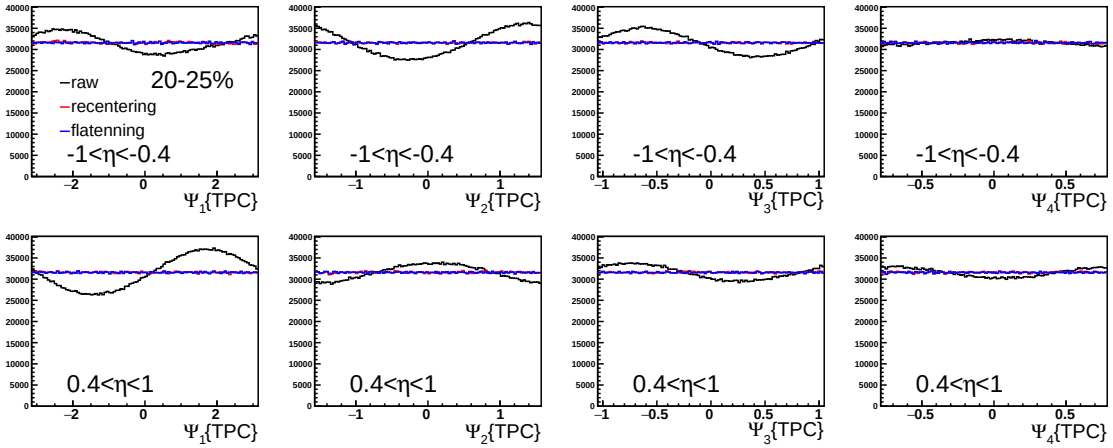

Fig. 7: First-, second-, third-, and fourth-order event plane distributions reconstructed by TPC in two different sub events ($-1 < \eta < 0.4$, $0.4 < \eta < 1$) before and after the calibration in 20-25% centrality.

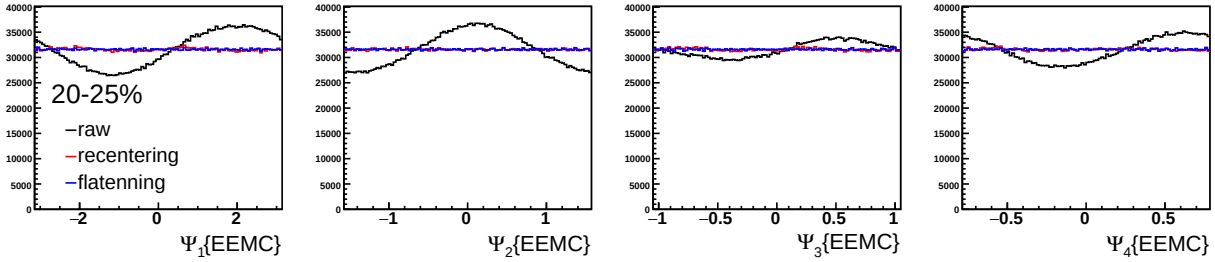

Fig. 8: First-, second-, third-, and fourth-order event plane distributions reconstructed by EEMC before and after the calibration in 20-25% centrality.

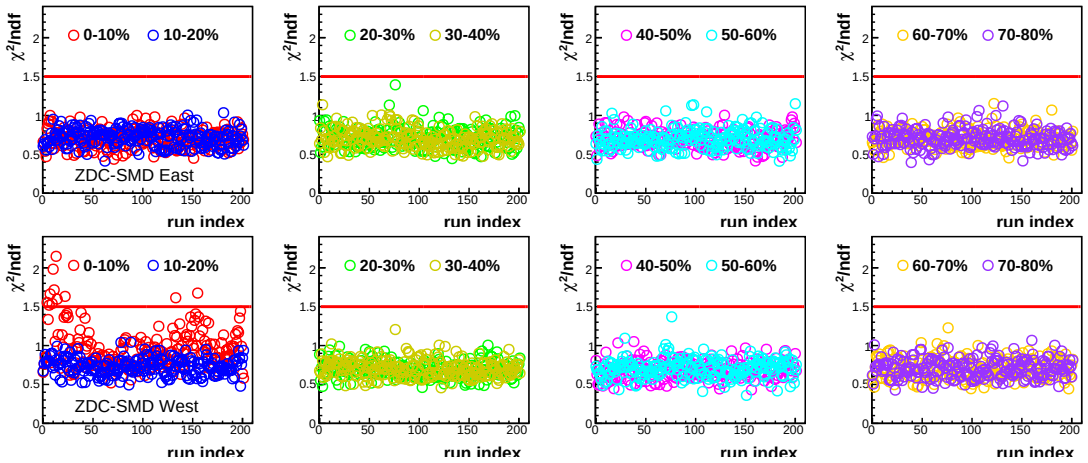

Fig. 9: χ^2/NDF from the constant fitting to the event plane distributions of ZDC-SMD as a function of run index.

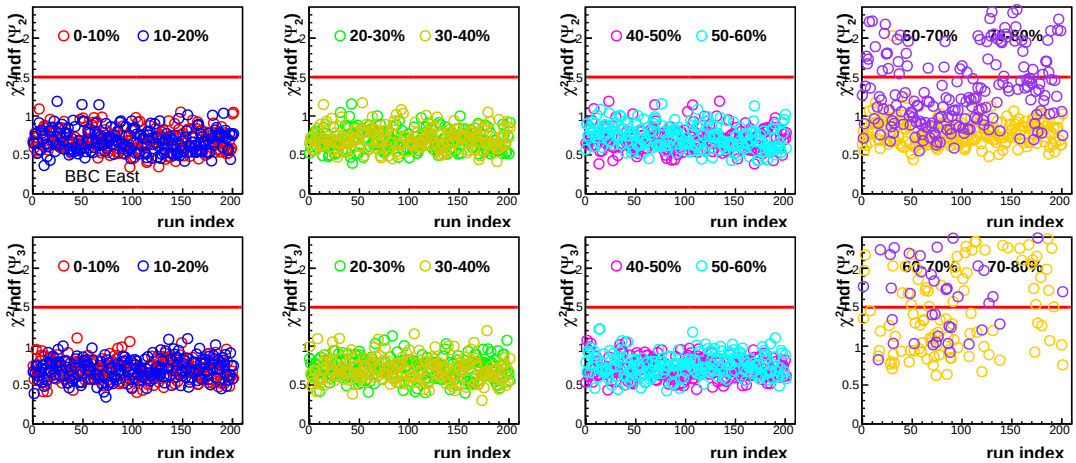

Fig. 10: χ^2/NDF from the constant fitting to the event plane distributions of BBC East as a function of run index.

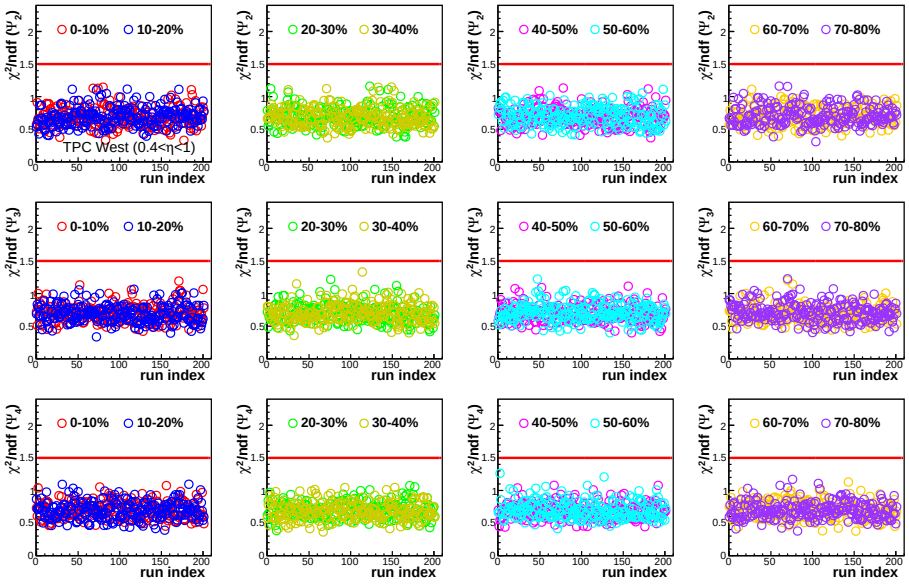

Fig. 11: χ^2/NDF from the constant fitting to the event plane distributions of TPC West as a function of run index.

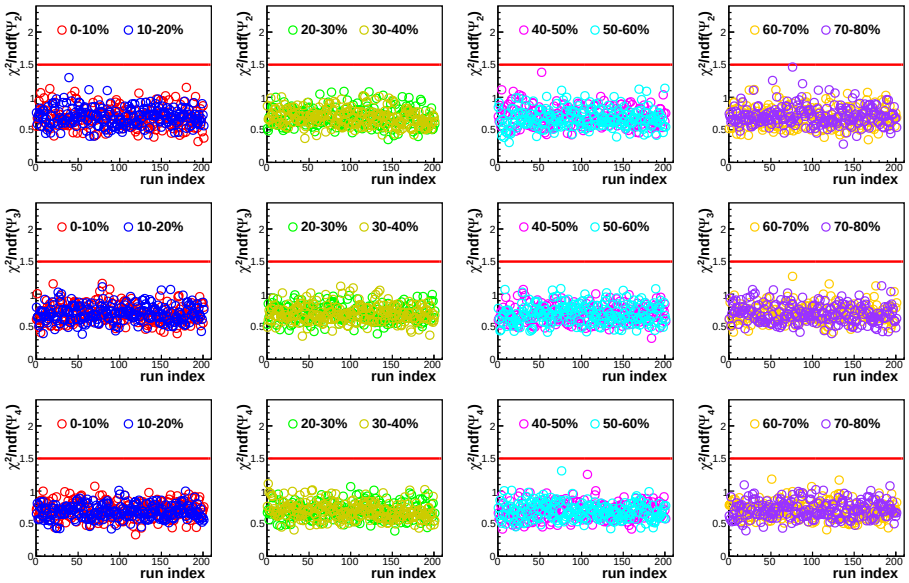

Fig. 12: χ^2/NDF from the constant fitting to the event plane distributions of EEMC (West side) as a function of run index.

2.4.3 Event plane resolution

Event plane resolutions were estimated via 3 sub event method [4, 5]:

$$\mathrm{Res}\{\Psi_n^A\} = \sqrt{\frac{\langle \cos n(\Psi_n^A - \Psi_n^B)\rangle \langle \cos n(\Psi_n^A - \Psi_n^C)\rangle}{\langle \cos n(\Psi_n^B - \Psi_n^C)\rangle}} \tag{4}$$

where A-C denote sub-events in East (Au-going) or West (Cu-going) sides. Figure 13 shows the event plane correlations between the same detectors at forward and backward rapidities, where filled symbols show cosine term and open symbols show sine term. BBC event plane can be used up to the second-order and TPC event plane can be used up to fourth-order.

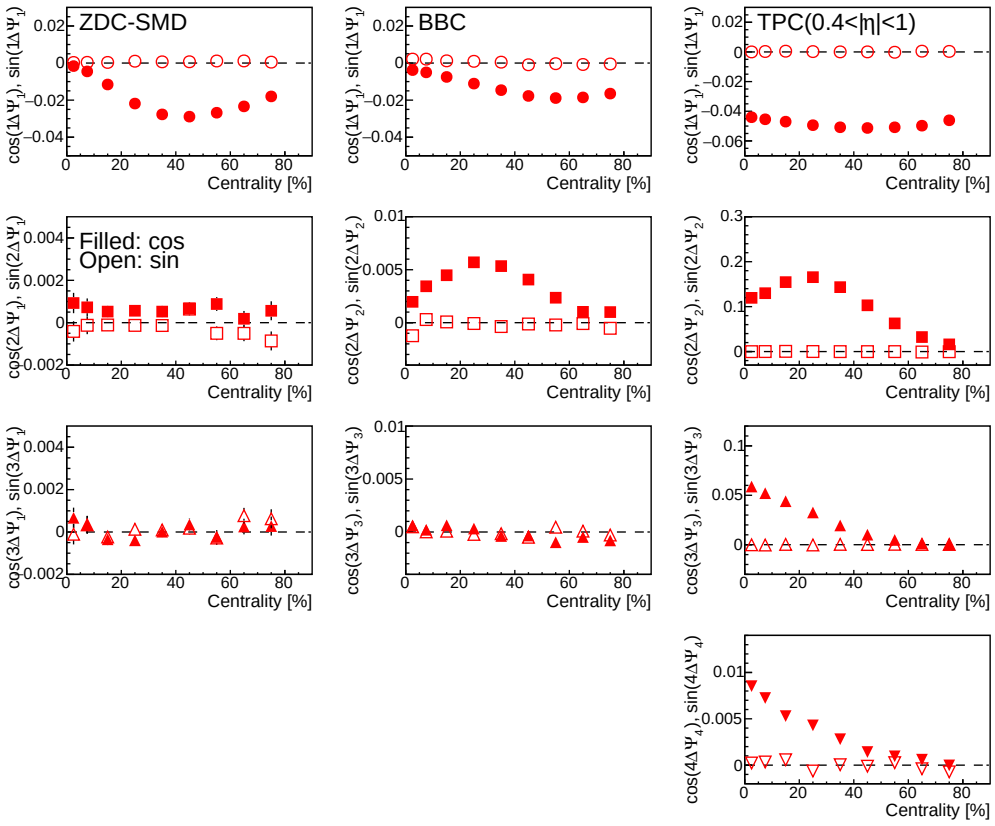

Fig. 13: Event plane correlations between the same detectors at forward and backward directions.

To estimate the event plane resolution of ZDC-SMD, the first-order event plane correlations between ZDC-SMD and other detectors were checked in Fig. 15. Since the correlation with BBC is largest, one of BBCs was used to estimate the resolution in this analysis. Figure 15 shows the event plane resolution of ZDC-SMD via 3 sub-events method with BBC-East.

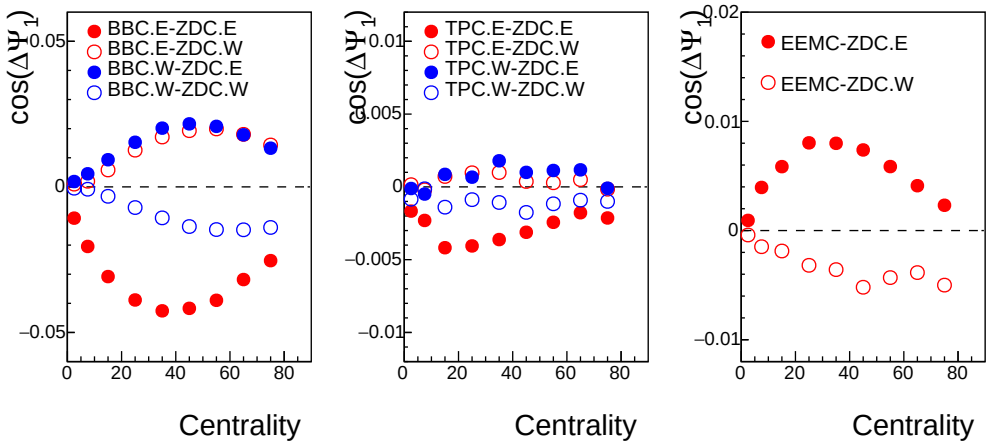

Fig. 14: First-order event plane correlations between ZDC-SMD and other detectors.

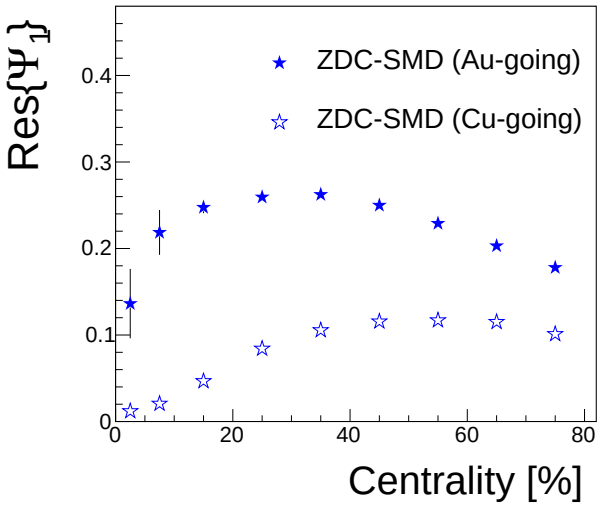

Fig. 15: Event plane resolution of ZDC-SMD plane

2.5 Directed flow measurements

Directed flow v_1 was measured with the event plane method using the spectator plane determined by ZDC-SMD in Au-going side:

$$v_1\{\mathrm{ZDC}\} = \frac{\langle \cos(\phi - \Psi_1) \rangle}{\mathrm{Res}\{\Psi_1\}} \tag{5}$$

where ϕ denotes the azimuthal angle of particles and $\langle\,\rangle$ means average over all particles in all events. By using the spectator plane, the non-flow effect like momentum conservation would be minimized. In this analysis, v_1 is measured in $\eta < 1$ without the sign flipping at the backward rapidity.

2.6 Trigger efficiency correction

Trigger efficiency was corrected when measuring v_1 and the event plane correlations used for the estimate of event plane resolution. Figure 16 shows the correction factor for each z-vertex bin, which was obtained by taking the ratio of RefMult distribution after the correction of luminosity dependence and Glauber+NBD fitting function to it. The correction factor was used as a weight when filling v_1 or the event plane correlations to TProfile.

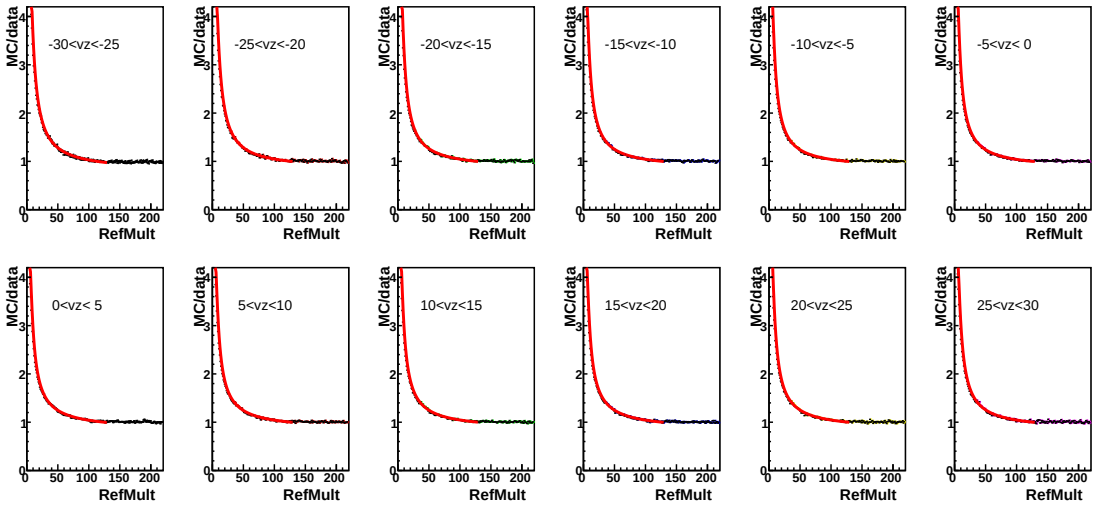

Fig. 16: The correction factor of trigger bias for each z-vertex bin

2.7 Systematic uncertainties

Systematic uncertainties were estimated by the variations of track quality cut and z-vertex cut. Also, the uncertainty of the event plane resolution was taken into account by

using different combinations of 3-sub events. The source of the systematic uncertainties are listed below:

- dca<3 cm or dca<2 cm
- nHitsFit>15 or nHitsFit>20
- $|v_z|$ <30 cm or $|v_z|$ <20 cm
- 3-sub combinations for the estimate of event plane resolution:
  (ZDCE, BBCE, ZDCW) or (ZDCE, BBCW, ZDCW) or (ZDCE, EEMC, ZDCW)

Figure 17 and 18 show $v_1(p_T)$ and Fig. 19 shows the difference of v_1 between positive and negative charged particles, where one of sources of the systematic uncertainties is varied.

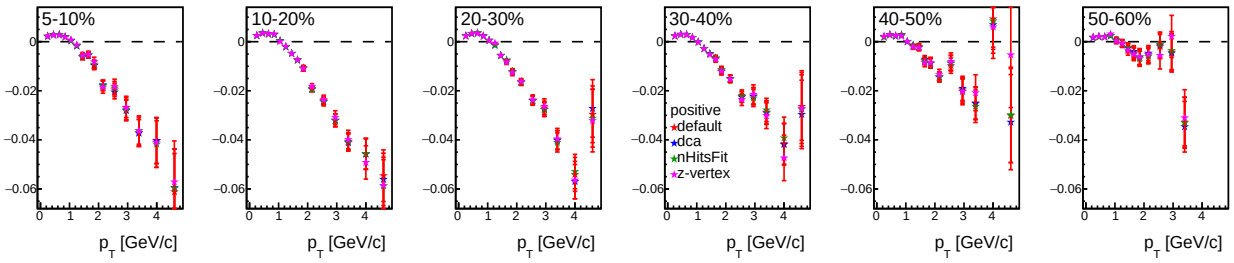

Fig. 17: v_1 of positive charged particles as a function of p_T when varying the systematic source.

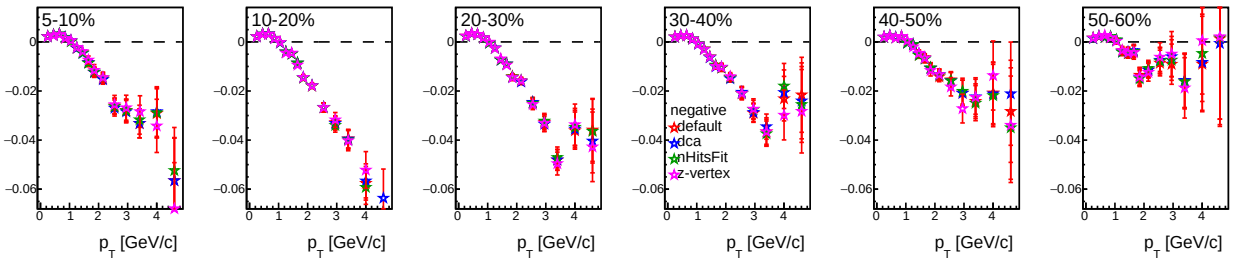

Fig. 18: v_1 of negative charged particles as a function of p_T when varying the systematic source.

Figure 22 shows the event plane resolution of $\Psi_1\{\text{ZDC}\}$ in Au-going side. In 3-sub event method, the estimated resolution changes if the third sub event except ZDCs is changed. In estimating the resolution of ZDC.E, the resolution become better (worse) if we use the BBC in the same (opposite) angle. This might be related to the event plane decorrelation. In this analysis, the difference was included into the systematic

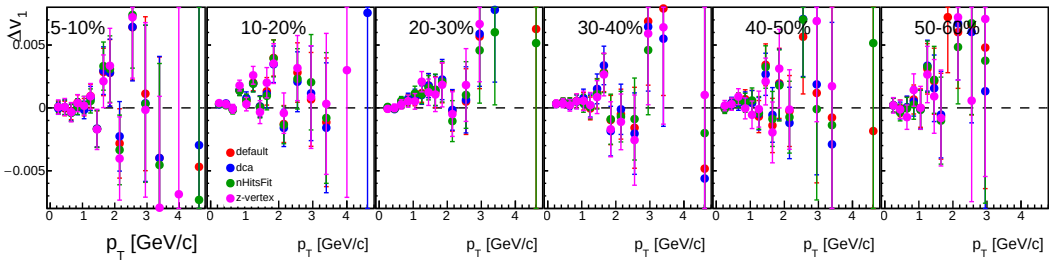

Fig. 19: Δv_1 between positive and negative charged particles as a function of p_T when varying the systematic source.

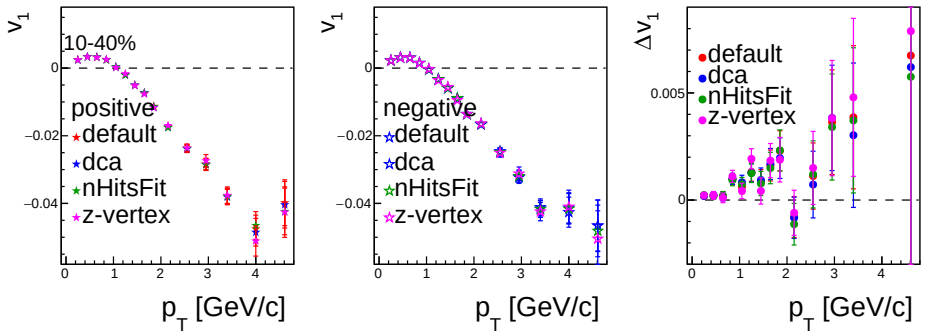

Fig. 20: v_1 and Δv_1 as a function of p_T in 10-40% centrality when varying the systematic source.

uncertainty. This effect makes v_1 move to the same direction. Figure 23 and 24 show the comparison of v_1 between different 3sub combinations.

Final systematic uncertainties are defined as a quadratic sum of the difference from the default cut condition. But for the uncertainty of event plane resolution the corrected v_1 moves to the same direction by the same fraction. Therefore it will be plotted separately in final figures.

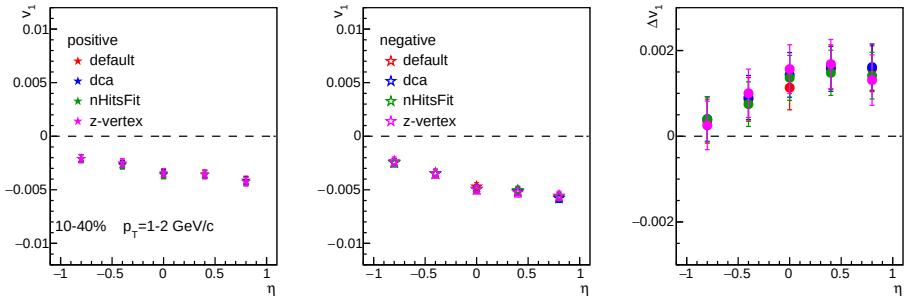

Fig. 21: v_1 and Δv_1 as a function of η in 10-40% centrality when varying the systematic source.

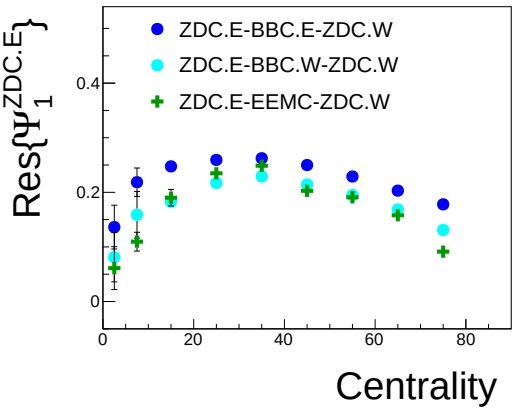

Fig. 22: Resolution of first-order event plane of ZDC-SMD east in Au-going side

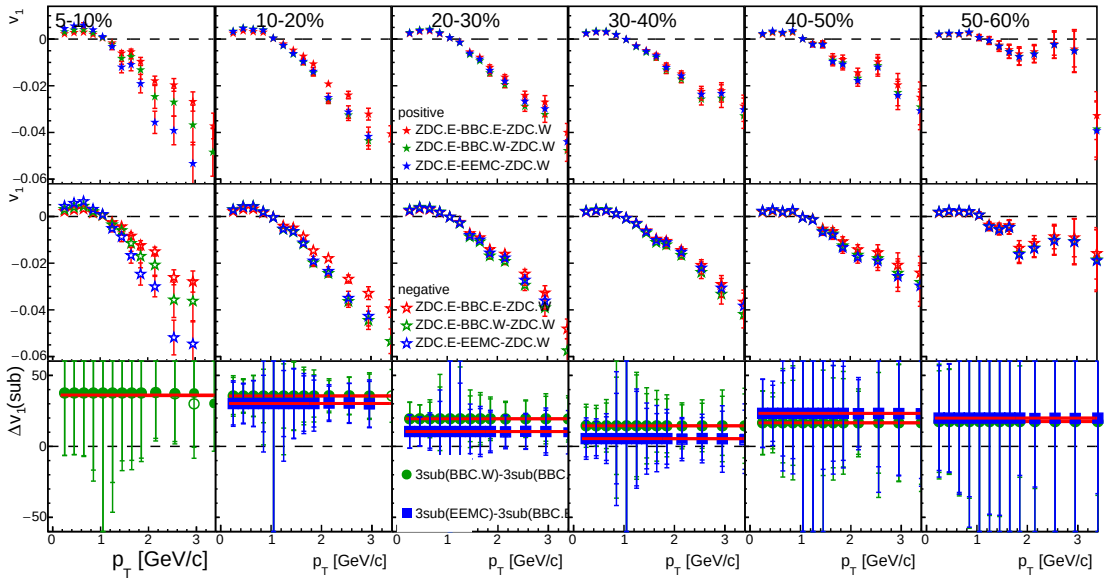

Fig. 23: v_1 and Δv_1 as a function of p_T using different 3sub combinations, where Δv_1 shows the difference of v_1 between 3sub combinations for the same charged particles.

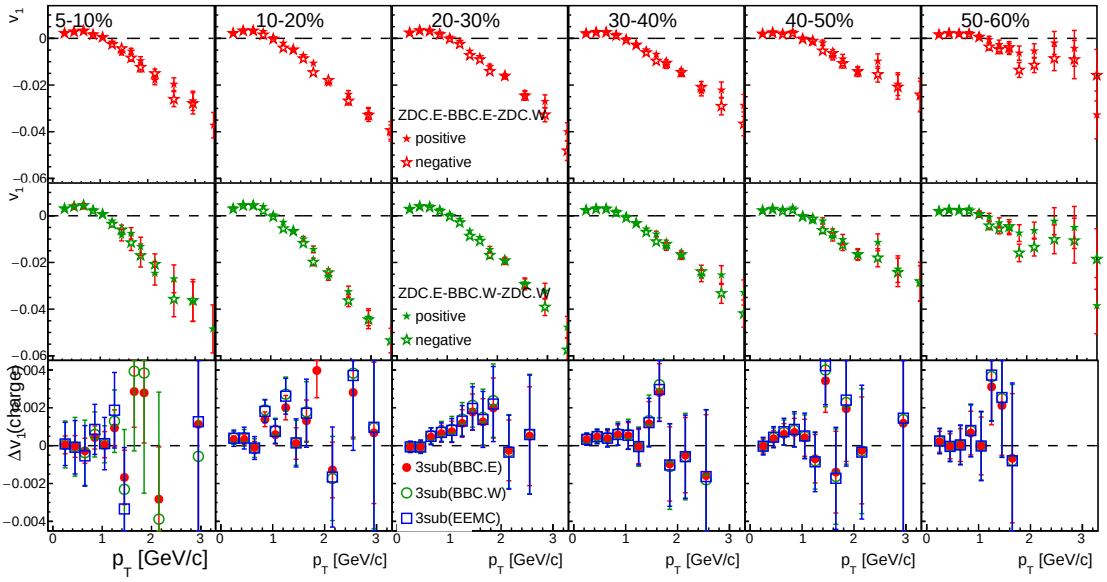

Fig. 24: v_1 and Δv_1 as a function of p_T using different 3 sub combinations, where Δv_1 shows the difference of v_1 between charges for different 3 sub combinations.

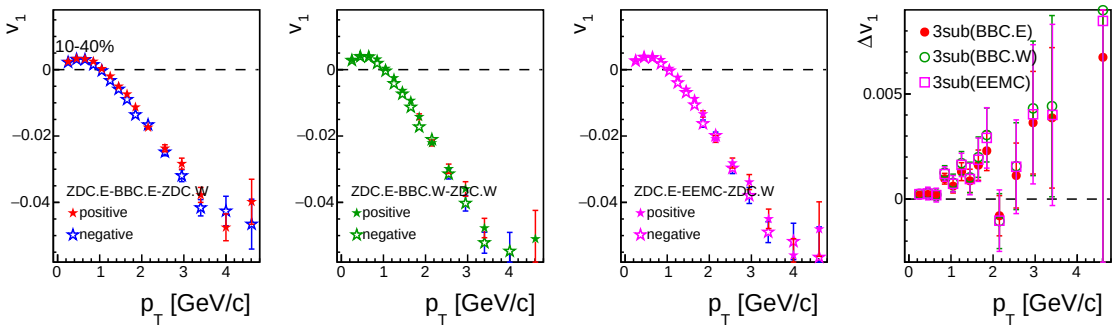

Fig. 25: v_1 and Δv_1 in 10-40% centrality as a function of p_T using different 3 sub combinations, where Δv_1 shows the difference of v_1 between charges for different 3 sub combinations.

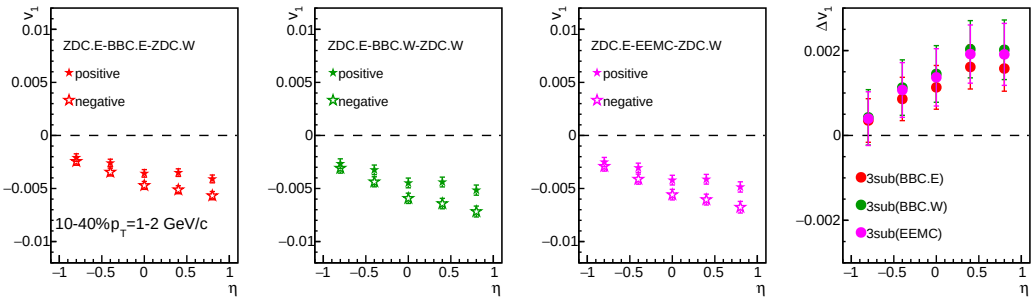

Fig. 26: v_1 and Δv_1 in 10-40% centrality as a function of η using different 3 sub combinations, where Δv_1 shows the difference of v_1 between charges for different 3 sub combinations.

3 Results

3.1 Final figures

Figure 27 shows v_1 as a function of p_T for 10 % centrality step with the systematic uncertainties. The v_1 is measured with respect to the spectator plane determined by ZDC-SMD in Au-going side ($\eta < 0$), but the sign of v_1 is defined to be positive at $\eta > 0$ (Cu-going side) to follow the convention. Lower panes of the figure shows Δv_1 defined as the difference between positive and negative charged particles ($v_1(h+) - v_1(h-)$). Figure 28 shows $v_1(p_T)$ and $\Delta v_1(p_T)$ for 10-40% centrality bin. The Δv_1 has finite value (10% of v_1 signal) and looks to slightly increase with p_T in p_T <2 GeV/c. The PHSD model calculations with and without the initial electric field (EF) [2] are plotted together. The model assumes that the all electric charges are affected by EF and therefore shows large separation of v_1 between positive and negative particles. Just for comparison, Δv_1 from the model with EF is scaled by 0.1. The p_T dependence of Δv_1 looks similar to the data.

The v_1 and Δv_1 for Au+Au collisions were also measured for the comparison (see the detail in Sec. B), where the even component of v_1 was measured. Figure 29 shows the comparison between Cu+Au and Au+Au collisions. The magnitude of v_1 in Au+Au collisions is much smaller than that in Cu+Au collisions because the v_1 in Au+Au is only due to the density fluctuation of participants. The Δv_1 in Au+Au is consistent with zero within the systematic uncertainty.

Figure 30 shows η dependence of v_1 and Δv_1 in 10-40% centrality. We naively expect the larger electric field in Au-going direction (backward) than that in Cu-going direction (forward) which may lead to different Δv_1 between forward and backward rapidities. But the Δv_1 slightly increases when going to forward direction which is the opposite trend to our expectation and also the PHSD model prediction.

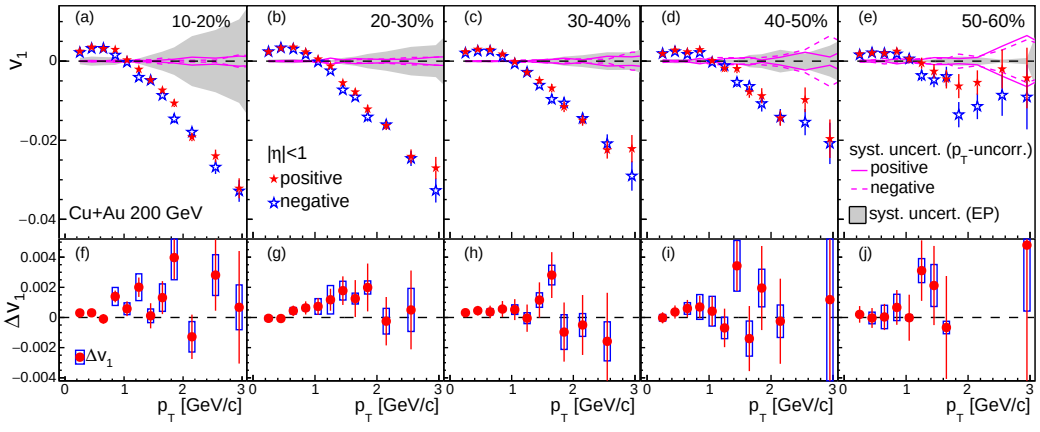

Fig. 27: v_1 and Δv_1 as a function of p_T for five centrality bins

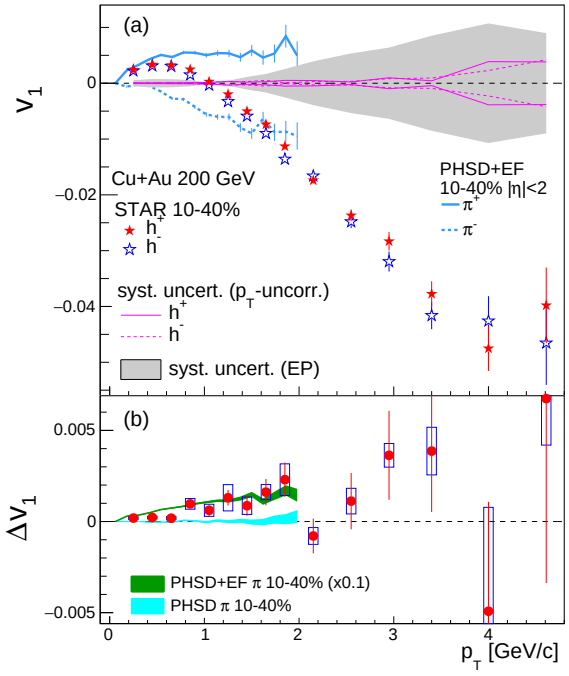

Fig. 28: v_1 and Δv_1 as a function of p_T in 10-40% centrality. The PHSD model calculations with and without the initial electric filed (EF) are compared, where the Δv_1 from the model with EF is scaled by 0.1.

3.2 Comparison with PHENIX

Recently PHENIX submitted a paper on Cu+Au flow [7] in arXiv, where charge combined v_1 is presented. Our results are compared to the PHENIX results in Figure 31 and are consistent with each other within their systematic uncertainties.

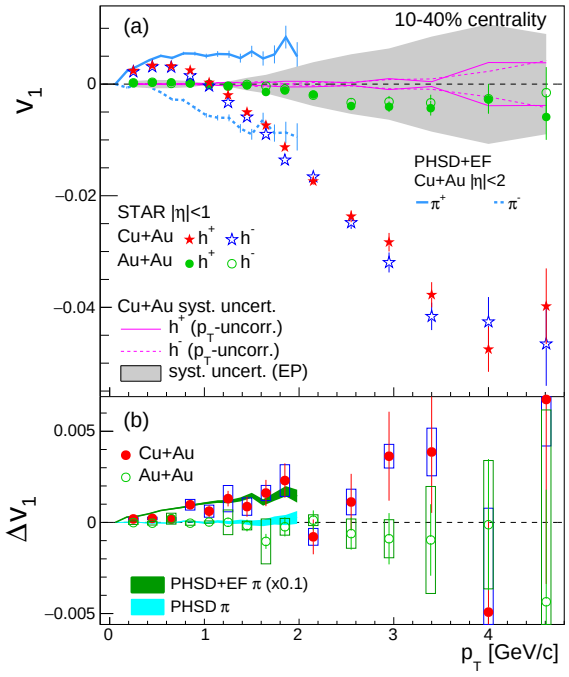

Fig. 29: v_1 and Δv_1 as a function of p_T in 10-40% centrality in Cu+Au and Au+Au collisions. The PHSD model calculations with and without the initial electric filed (EF) are compared, where the Δv_1 from the model with EF is scaled by 0.1.

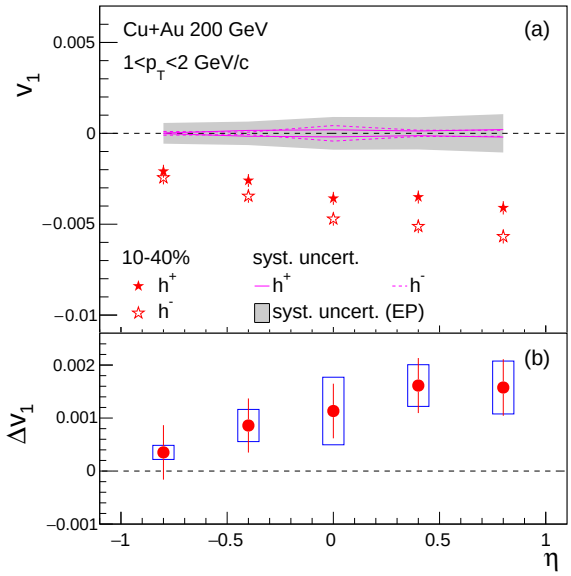

Fig. 30: v_1 and Δv_1 as a function of η in 10-40% centrality.

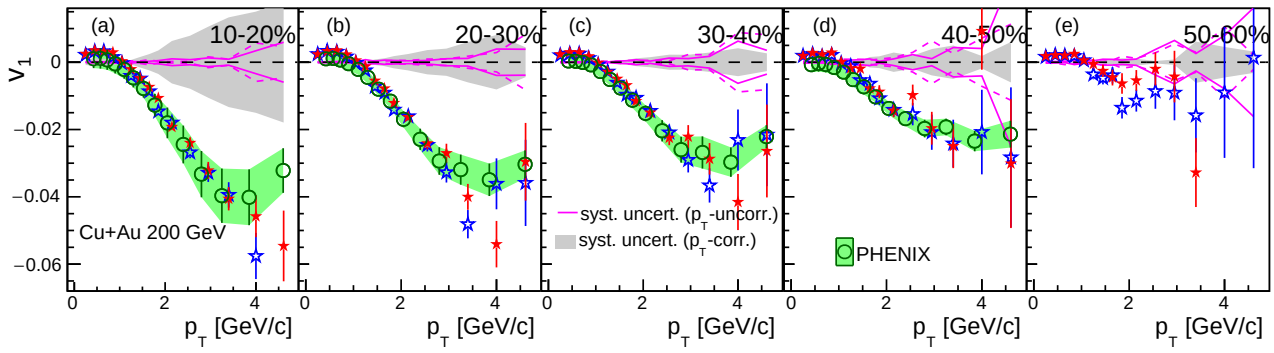

Fig. 31: Comparison of $v_1(p_T)$ with the PHENIX results

A Data table

Table 2: $v_1(p_T)$ of positve charged particles in centrality 10-20%

$p_T(GeV/c)$	v_1	stat.uncert.	syst.uncert.(p_T-uncorr.)	syst.uncert.(p_T-corr.)
0.25	0.0025	0.00016	9e-05	0.00082
0.45	0.00353	0.00019	0.00018	0.00116
0.65	0.00315	0.00022	8e-05	0.00104
0.85	0.00293	0.00028	0.00026	0.00096
1.05	0.0003	0.00034	0.0002	0.0001
1.25	-0.00205	0.00044	0.0002	0.00068
1.45	-0.00474	0.00058	0.00011	0.00156
1.65	-0.00733	0.00075	0.00029	0.00241
1.85	-0.01062	0.00097	0.00048	0.00349
2.15	-0.01922	0.00101	0.001	0.00631
2.55	-0.02397	0.0016	0.00076	0.00788
2.95	-0.03215	0.00253	0.00128	0.01056
3.4	-0.04057	0.00346	0.00089	0.01333
4	-0.04578	0.0062	0.00341	0.01504
4.61	-0.05459	0.01051	0.00593	0.01793

Table 3: $v_1(p_T)$ of positve charged particles in centrality 20-30%

$p_T(GeV/c)$	v_1	stat.uncert.	syst.uncert.(p_T-uncorr.)	syst.uncert.(p_T-corr.)
0.25	0.00234	0.00016	3e-05	0.00035
0.45	0.0033	0.00019	0.00013	0.00049
0.65	0.00353	0.00024	0.00019	0.00053
0.85	0.00232	0.00031	0.00011	0.00035
1.05	0.00053	0.00039	0.00014	8e-05
1.25	-0.00125	0.00051	0.00076	0.00019
1.45	-0.00548	0.00066	0.00032	0.00082
1.65	-0.00778	0.00084	0.00064	0.00117
1.85	-0.01211	0.00109	0.00053	0.00181
2.15	-0.01631	0.0011	0.00041	0.00244
2.55	-0.02409	0.00178	0.00052	0.00361
2.95	-0.02702	0.00281	0.00104	0.00405
3.4	-0.03999	0.00385	0.00114	0.00599
4	-0.05406	0.0069	0.00392	0.00809
4.61	-0.02957	0.01155	0.00385	0.00443

Table 4: $v_1(p_T)$ of positve charged particles in centrality 30-40%

$p_T(GeV/c)$	v_1	stat.uncert.	syst.uncert.(p_T-uncorr.)	syst.uncert.(p_T-corr.)
0.25	0.00237	0.00019	9e-05	0.00024
0.45	0.00299	0.00022	7e-05	0.0003
0.65	0.00293	0.00029	0.00011	0.00029
0.85	0.00177	0.00037	6e-05	0.00018
1.05	-0.00015	0.00049	8e-05	2e-05
1.25	-0.00283	0.00063	9e-05	0.00028
1.45	-0.00491	0.00081	0.00033	0.00049
1.65	-0.00682	0.00105	0.00043	0.00068
1.85	-0.01153	0.00135	0.00074	0.00115
2.15	-0.01496	0.00136	0.00034	0.0015
2.55	-0.02244	0.0022	0.00123	0.00224
2.95	-0.02213	0.00345	0.00108	0.00221
3.4	-0.0287	0.00469	0.00174	0.00287
4	-0.04153	0.00833	0.00627	0.00415
4.61	-0.02637	0.01379	0.00354	0.00264

Table 5: $v_1(p_T)$ of positve charged particles in centrality 40-50%

$p_T(GeV/c)$	v_1	stat.uncert.	syst.uncert.(p_T-uncorr.)	syst.uncert.(p_T-corr.)
0.25	0.0019	0.00026	0.00033	0.00038
0.45	0.00277	0.00031	0.00013	0.00055
0.65	0.00233	0.0004	0.00019	0.00047
0.85	0.00288	0.00052	0.00068	0.00057
1.05	0.00012	0.00068	0.00018	2e-05
1.25	-0.00182	0.00089	0.00064	0.00037
1.45	-0.00189	0.00115	0.00073	0.00038
1.65	-0.00777	0.00149	0.00099	0.00155
1.85	-0.00876	0.00192	0.00029	0.00175
2.15	-0.01439	0.00194	0.00099	0.00287
2.55	-0.00975	0.00311	0.00226	0.00195
2.95	-0.0196	0.00487	0.00105	0.00391
3.4	-0.02492	0.00654	0.00436	0.00497
4	0.00928	0.0115	0.00408	0.00185
4.61	-0.03011	0.01916	0.02492	0.00601

Table 6: $v_1(p_T)$ of positve charged particles in centrality 50-60%

$p_T(GeV/c)$	v_1	stat.uncert.	syst.uncert.(p_T-uncorr.)	syst.uncert.(p_T-corr.)
0.25	0.00181	0.00039	0.00021	0.00034
0.45	0.00208	0.00046	0.00022	0.00039
0.65	0.00199	0.00061	9e-05	0.00037
0.85	0.00249	0.00081	0.00071	0.00047
1.05	0.00056	0.00107	0.00031	0.0001
1.25	-0.0005	0.0014	0.00044	0.0001
1.45	-0.00257	0.00182	0.00088	0.00048
1.65	-0.00453	0.00236	0.00085	0.00085
1.85	-0.00631	0.00305	0.00064	0.00118
2.15	-0.00539	0.00308	0.00093	0.00101
2.55	-0.00197	0.00492	0.00379	0.00037
2.95	-0.00426	0.00767	0.00647	0.0008
3.4	-0.03277	0.01025	0.00259	0.00613
4	0.02426	0.01792	0.00793	0.00454
4.61	0.01699	0.02954	0.01616	0.00318

Table 7: $v_1(p_T)$ of negative charged particles in centrality 10-20%

$p_T(GeV/c)$	v_1	stat.uncert.	syst.uncert.(p_T-uncorr.)	syst.uncert.(p_T-corr.)
0.25	0.00219	0.00015	3e-05	0.00072
0.45	0.00322	0.00018	0.00011	0.00106
0.65	0.00325	0.00023	8e-05	0.00107
0.85	0.00154	0.00027	0.00013	0.00051
1.05	-0.00027	0.00035	0.00016	9e-05
1.25	-0.00406	0.00047	0.00041	0.00134
1.45	-0.00485	0.0006	0.00037	0.0016
1.65	-0.00864	0.0008	0.00078	0.00284
1.85	-0.01459	0.00106	0.00023	0.0048
2.15	-0.01793	0.00106	0.00022	0.00589
2.55	-0.02678	0.00174	0.00027	0.0088
2.95	-0.03282	0.00274	0.0016	0.01078
3.4	-0.03942	0.00377	0.0009	0.01295
4	-0.05757	0.00685	0.00571	0.01891
4.61	-0.0681	0.01166	0.00465	0.02237

Table 8: $v_1(p_T)$ of negative charged particles in centrality 20-30%

$p_T(GeV/c)$	v_1	stat.uncert.	syst.uncert.(p_T-uncorr.)	syst.uncert.(p_T-corr.)
0.25	0.0024	0.00016	0.00014	0.00036
0.45	0.00337	0.00019	6e-05	0.0005
0.65	0.00308	0.00024	5e-05	0.00046
0.85	0.00168	0.00031	5e-05	0.00025
1.05	-0.00019	0.0004	0.00037	3e-05
1.25	-0.00242	0.00052	0.00024	0.00036
1.45	-0.00726	0.00069	0.00041	0.00109
1.65	-0.00904	0.00089	0.00035	0.00135
1.85	-0.0141	0.00115	0.00051	0.00211
2.15	-0.01607	0.00117	0.00054	0.00241
2.55	-0.02459	0.00191	0.00093	0.00368
2.95	-0.03269	0.00305	0.00097	0.0049
3.4	-0.04812	0.0042	0.00179	0.0072
4	-0.03612	0.00757	0.00287	0.00541
4.61	-0.03585	0.01281	0.00824	0.00537

Table 9: $v_1(p_T)$ of negative charged particles in centrality 30-40%

$p_T(GeV/c)$	v_1	stat.uncert.	syst.uncert.(p_T-uncorr.)	syst.uncert.(p_T-corr.)
0.25	0.00205	0.00019	8e-05	0.0002
0.45	0.00254	0.00022	9e-05	0.00025
0.65	0.00256	0.00029	9e-05	0.00026
0.85	0.00121	0.00038	5e-05	0.00012
1.05	-0.00067	0.0005	0.00026	7e-05
1.25	-0.00279	0.00065	0.0003	0.00028
1.45	-0.00607	0.00085	0.00028	0.00061
1.65	-0.00964	0.0011	0.00051	0.00096
1.85	-0.01057	0.00142	0.00043	0.00106
2.15	-0.01447	0.00145	0.00057	0.00145
2.55	-0.02085	0.00235	0.00044	0.00208
2.95	-0.02902	0.00373	0.00227	0.0029
3.4	-0.0366	0.00509	0.00222	0.00366
4	-0.02311	0.00907	0.00884	0.00231
4.61	-0.02154	0.01528	0.00815	0.00215

Table 10: $v_1(p_T)$ of negative charged particles in centrality 40-50%

$p_T(GeV/c)$	v_1	stat.uncert.	syst.uncert.(p_T-uncorr.)	syst.uncert.(p_T-corr.)
0.25	0.00192	0.00026	0.00012	0.00038
0.45	0.00241	0.00031	0.00015	0.00048
0.65	0.00174	0.0004	0.00019	0.00035
0.85	0.00218	0.00053	0.00014	0.00043
1.05	-0.00029	0.0007	0.0009	6e-05
1.25	-0.00113	0.00092	0.00089	0.00023
1.45	-0.00532	0.0012	0.00086	0.00106
1.65	-0.00637	0.00156	0.00063	0.00127
1.85	-0.01071	0.00202	0.00092	0.00214
2.15	-0.01414	0.00205	0.00138	0.00282
2.55	-0.01541	0.00332	0.00292	0.00308
2.95	-0.02079	0.00523	0.0064	0.00415
3.4	-0.02415	0.00708	0.00257	0.00482
4	-0.02074	0.01257	0.00715	0.00414
4.61	-0.02827	0.02081	0.01131	0.00564

Table 11: $v_1(p_T)$ of negative charged particles in centrality 50-60%

$p_T(GeV/c)$	v_1	stat.uncert.	syst.uncert.(p_T-uncorr.)	syst.uncert.(p_T-corr.)
0.25	0.0016	0.00039	0.00021	0.0003
0.45	0.00211	0.00047	0.00029	0.00039
0.65	0.00196	0.00062	0.00071	0.00037
0.85	0.00182	0.00082	0.00043	0.00034
1.05	0.00058	0.00109	0.00044	0.00011
1.25	-0.00361	0.00144	0.00065	0.00068
1.45	-0.00469	0.00189	0.00073	0.00088
1.65	-0.00387	0.00246	0.00058	0.00073
1.85	-0.01352	0.00319	0.00179	0.00253
2.15	-0.01142	0.00324	0.00115	0.00214
2.55	-0.00859	0.00523	0.00281	0.00161
2.95	-0.00906	0.00819	0.00543	0.0017
3.4	-0.01577	0.01102	0.00297	0.00295
4	-0.00898	0.01944	0.0105	0.00168
4.61	0.00134	0.03283	0.00212	0.00025

Table 12: $\Delta v_1(p_T)$ in centrality 10-20%

$p_T(GeV/c)$	Δv_1	stat.uncert.	syst.uncert.
0.25	0.0003	0.00022	0.00013
0.45	0.00031	0.00026	0.00015
0.65	-8e-05	0.00032	8e-05
0.85	0.00139	0.00039	0.0006
1.05	0.00058	0.00049	0.00039
1.25	0.00201	0.00064	0.00089
1.45	0.00011	0.00083	0.00045
1.65	0.00132	0.00109	0.00091
1.85	0.00397	0.00144	0.00147
2.15	-0.00127	0.00147	0.00101
2.55	0.00281	0.00236	0.00135
2.95	0.00068	0.00373	0.00149
3.4	-0.00114	0.00512	0.0016
4	0.01179	0.00924	0.00982
4.61	0.01351	0.01569	0.0087

Table 13: $\Delta v_1(p_T)$ in centrality 20-30%

$p_T(GeV/c)$	Δv_1	stat.uncert.	syst.uncert.
0.25	-5e-05	0.00023	0.00016
0.45	-6e-05	0.00027	8e-05
0.65	0.00045	0.00034	0.00021
0.85	0.00063	0.00044	0.00017
1.05	0.00073	0.00056	0.00052
1.25	0.00118	0.00073	0.00094
1.45	0.00178	0.00095	0.00062
1.65	0.00125	0.00123	0.00036
1.85	0.00199	0.00159	0.00044
2.15	-0.00024	0.00161	0.00085
2.55	0.0005	0.00261	0.00143
2.95	0.00567	0.00415	0.00172
3.4	0.00813	0.0057	0.00307
4	-0.01792	0.01025	0.00648
4.61	0.00627	0.01725	0.00828

Table 14: $\Delta v_1(p_T)$ in centrality 30-40%

$p_T(GeV/c)$	Δv_1	stat.uncert.	syst.uncert.
0.25	0.00032	0.00027	4e-05
0.45	0.00045	0.00032	0.0001
0.65	0.00037	0.00041	0.0002
0.85	0.00056	0.00053	0.00011
1.05	0.00052	0.0007	0.00032
1.25	-4e-05	0.00091	0.00036
1.45	0.00116	0.00117	0.00048
1.65	0.00281	0.00152	0.00065
1.85	-0.00096	0.00196	0.00115
2.15	-0.00049	0.00199	0.00076
2.55	-0.00157	0.00322	0.0013
2.95	0.00689	0.00508	0.00263
3.4	0.00791	0.00692	0.00333
4	-0.01841	0.01232	0.0045
4.61	-0.00482	0.02058	0.00657

Table 15: $\Delta v_1(p_T)$ in centrality 40-50%

$p_T(GeV/c)$	Δv_1	stat.uncert.	syst.uncert.
0.25	-1e-05	0.00037	0.00022
0.45	0.00036	0.00043	0.00012
0.65	0.0006	0.00057	0.00039
0.85	0.0007	0.00074	0.00082
1.05	0.00042	0.00098	0.00099
1.25	-0.00068	0.00128	0.00071
1.45	0.00343	0.00166	0.00168
1.65	-0.00139	0.00216	0.00117
1.85	0.00195	0.00279	0.00125
2.15	-0.00024	0.00282	0.00108
2.55	0.00566	0.00455	0.00511
2.95	0.00118	0.00715	0.00591
3.4	-0.00076	0.00964	0.00334
4	0.03003	0.01704	0.01207
4.61	-0.00183	0.02829	0.03273

Table 16: $\Delta v_1(p_T)$ in centrality 50-60%

$p_T(GeV/c)$	Δv_1	stat.uncert.	syst.uncert.
0.25	0.00021	0.00055	4e-05
0.45	-2e-05	0.00066	0.00039
0.65	3e-05	0.00087	0.00078
0.85	0.00067	0.00115	0.00087
1.05	-1e-05	0.00153	0.00018
1.25	0.00311	0.00201	0.0008
1.45	0.00212	0.00263	0.00139
1.65	-0.00065	0.00342	0.00041
1.85	0.00722	0.00442	0.00198
2.15	0.00602	0.00447	0.00213
2.55	0.00662	0.00719	0.0062
2.95	0.0048	0.01122	0.00437
3.4	-0.01699	0.01505	0.00602
4	0.03325	0.02644	0.01161
4.61	0.01565	0.04416	0.01609

Table 17: v_1 of positve charged particles in centrality 10-40%

p_T (GeV/c)	v_1	stat.uncert.	syst.uncert.(p_T-uncorr.)	syst.uncert.(p_T-corr.)
0.25	0.00242	0.0001	5e-05	0.00055
0.45	0.00334	0.00012	6e-05	0.00075
0.65	0.00323	0.00014	8e-05	0.00073
0.85	0.00248	0.00018	0.0001	0.00056
1.05	0.00028	0.00023	0.00014	6e-05
1.25	-0.00196	0.00029	0.00034	0.00044
1.45	-0.00501	0.00038	0.00019	0.00113
1.65	-0.00737	0.0005	0.00028	0.00166
1.85	-0.01129	0.00064	0.00051	0.00255
2.15	-0.01739	0.00066	0.00048	0.00392
2.55	-0.02368	0.00105	0.00023	0.00534
2.95	-0.02831	0.00166	0.00098	0.00639
3.4	-0.03774	0.00226	0.00043	0.00851
4	-0.0475	0.00404	0.00387	0.01072
4.61	-0.03979	0.00678	0.00382	0.00898

Table 18: v_1 of negative charged particles in centrality 10-40%

p_T (GeV/c)	v_1	stat.uncert.	syst.uncert.(p_T-uncorr.)	syst.uncert.(p_T-corr.)
0.25	0.00223	0.0001	6e-05	0.0005
0.45	0.00312	0.00012	4e-05	0.0007
0.65	0.00304	0.00014	5e-05	0.00069
0.85	0.00151	0.00018	5e-05	0.00034
1.05	-0.00033	0.00023	0.00017	8e-05
1.25	-0.00327	0.00031	0.00031	0.00074
1.45	-0.00588	0.0004	0.00031	0.00133
1.65	-0.00898	0.00052	0.00052	0.00203
1.85	-0.01359	0.00069	7e-05	0.00306
2.15	-0.0166	0.00069	0.00029	0.00374
2.55	-0.0248	0.00113	0.00034	0.00559
2.95	-0.03195	0.00179	0.00082	0.0072
3.4	-0.0416	0.00246	0.00093	0.00938
4	-0.04258	0.00444	0.00228	0.0096
4.61	-0.04654	0.00752	0.00421	0.01049

Table 19: Δv_1 in centrality 10-40%

p_T (GeV/c)	Δv_1	stat.uncert.	syst.uncert.
0.25	0.00019	0.00014	7e-05
0.45	0.00022	0.00016	7e-05
0.65	0.00018	0.0002	8e-05
0.85	0.00097	0.00026	0.00029
1.05	0.00062	0.00033	0.00033
1.25	0.0013	0.00043	0.00072
1.45	0.00087	0.00055	0.00048
1.65	0.00161	0.00072	0.00042
1.85	0.0023	0.00094	0.00087
2.15	-0.00078	0.00096	0.00046
2.55	0.00112	0.00154	0.0007
2.95	0.00363	0.00244	0.00065
3.4	0.00386	0.00334	0.00131
4	-0.00491	0.006	0.0057
4.61	0.00675	0.01012	0.00255

Table 20: $v_1(\eta)$ of positve charged particles in centrality 10-40%

η	v_1	stat.uncert.	syst.uncert.(η-uncorr.)	syst.uncert.(η-corr.)
-0.8	-0.00208	0.00036	2e-05	0.00057
-0.4	-0.00258	0.00035	0.00016	0.00065
0	-0.00357	0.00036	0.00019	0.0009
0.4	-0.00349	0.00036	0.00013	0.00089
0.8	-0.00409	0.00037	0.0002	0.00106

Table 21: $v_1(\eta)$ of negative charged particles in centrality 10-40%

η	v_1	stat.uncert.	syst.uncert.(η-uncorr.)	syst.uncert.(η-corr.)
-0.8	-0.00243	0.00037	0.0001	0.00064
-0.4	-0.00344	0.00037	7e-05	0.00091
0	-0.0047	0.00037	0.00043	0.00122
0.4	-0.00511	0.00038	0.00017	0.0013
0.8	-0.00566	0.00039	0.00017	0.0015

Table 22: $\Delta v_1(\eta)$ in centrality 10-40%

η	Δv_1	stat.uncert.	syst.uncert.
-0.8	0.00035	0.00051	0.00013
-0.4	0.00086	0.00051	0.0003
0	0.00113	0.00052	0.00064
0.4	0.00161	0.00052	0.00039
0.8	0.00158	0.00053	0.0005

B Analysis in Au+Au collisions at $\sqrt{s_{NN}}$ = 200 GeV

In order to make a comparison with the v_1 results from Cu+Au collisions, the data of Au+Au collisions taken in Run10 was analyzed in the same way.

B.1 Event and track selection

The minimum bias trigger events triggered by vpd-mb was used, where only the data with the reversed field configuration (260021, 260031) were analyzed to be consistent with the analysis in Cu+Au collisions. The event cuts (zvertex cut and requrement from vpd-zvertex) and track selection cuts are the same as those in Cu+Au collisions.

Bad runs from RefMultCorr bad run list:
11044029 11047059 11047065 11047066 11047067 11048037 11049001 11049002 11049005 11049023 11051038 11051049 11051051 11051055 11051063 11051064 11051068 11052011 11053057 11054021 11054022 11054024 11054059 11054062 11054066 11057012 11057035 11057036 11058005 11058050 11058083 11059043 11059055 11059060 11059075 11059076 11059077 11060008 11060049 11060059 11060069 11060076 11061008 11061009 11061021 11061034 11061037 11061038 11061095 11063006 11063007 11063008 11063011 11063013 11063014 11063015 11063016 11063017 11063036 11063083 11064003 11064023 11065038 11066024 11066045 11071056 11072032 11072044 11072045 11073001 11073002 11073003 11073049 11075039 11075045 11075048

Bad runs from run QA:
11040085 11047045 11051037 11056020 11056022 11056036 11063040 11063047 11067024 11072030 11072031 11073004

B.2 Event plane determination

The first-order event plane was determined by ZDC-SMD as described in Section 2.4.1. Figure 32 show the resolution of Ψ_1 determined by ZDC-SMD East or West by using 3sub event method with BBC-East. In symmetric collisions, the resolutions of both sub detectors are supposed to be the same if both detetcors are identical and have the same performance. The evaluated resolution of ZDC.W is slightly lager than that of ZDC.E with this 3sub combination. If we assume both detectors are identical, the resolution can be estimated by 2sub event method, approximately by taking the square root of the event plane correlation between East and West. The resolution by 2sub event method is almost between the resolutions of ZDC.E and ZDC.W by 3sub event method. Figure 33 shows the resolutions of ZDC.E and ZDC.W by different 3sub combinations. If the BBC in the same side (East or West) as ZDC, the resolution of the ZDC become larger than using the BBC in the opposite side. These difference is included in the systematic uncertainty.

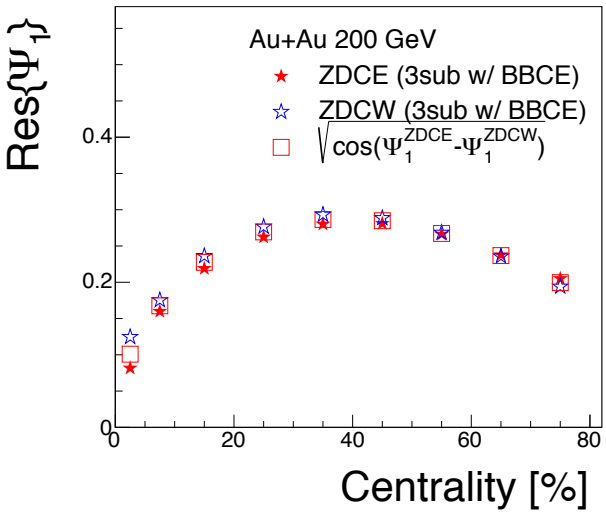

Fig. 32: Ψ_1 resolution of ZDC.E(W) estimated by 3 sub method using BBC-East in Au+Au collisions

B.3 Systematic checks

The systematics uncertainties were estimated with the same way in the analysis of Cu+Au collisions. Figure 34 shows $v_1^{\rm even}(p_T)$ of positively and negatively charged particles and its difference in 10-40% centrality when varying the zvertex and track selection cuts. Figure 35 shows $v_1^{\rm even}(p_T)$ of positively and negatively charged particles and its difference in 10-40% centrality when using different 3sub combinations in the estimate of the event plane resolution. Since the $v_1^{\rm even}$ signal in Au+Au collisions is much small, the effect from these 3sub combinations is relatively smaller than that for Cu+Au collisions. The event plane resolutions of ZDC.E and ZDC.W are comparable in Au+Au collisions unlike Cu+Au collisions. Therefore $v_1^{\rm even}$ can be measured using both event planes, which was checked as shown in Fig. 36. Both are consistent but the difference was included in the systematic uncertatinty, although it it small.

For the consistency check with the published result from the STAR, the η dependence of v_1 was compared with our result as shown in Fig. 37. The STAR published result uses both positively and negatively charged particles and the combined event plane of ZDC.E and ZDC.W. Our results are in good agreement with the published result.

B.4 Results

Figure 38 shows $v_1^{\rm even}$ as a function p_T in 10-40% in Au+Au collisions with the systematic uncertainty.

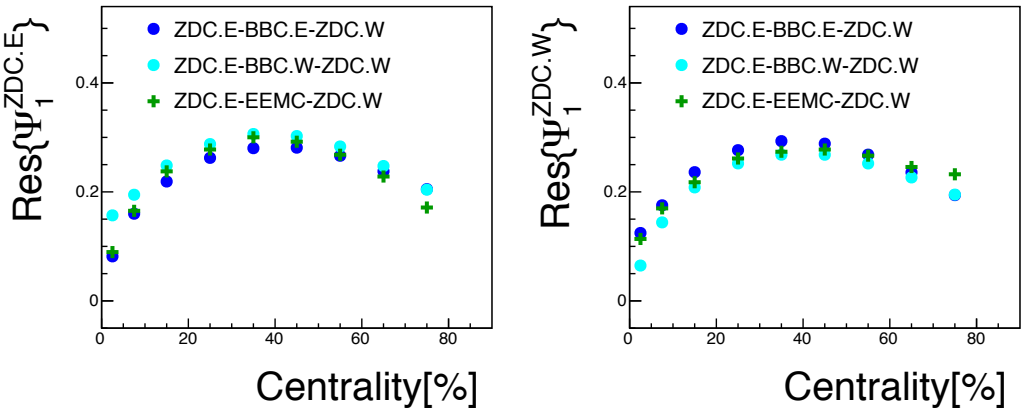

Fig. 33: Ψ_1 resolution of ZDC.E(W) with different 3 sub combinations in Au+Au collisions

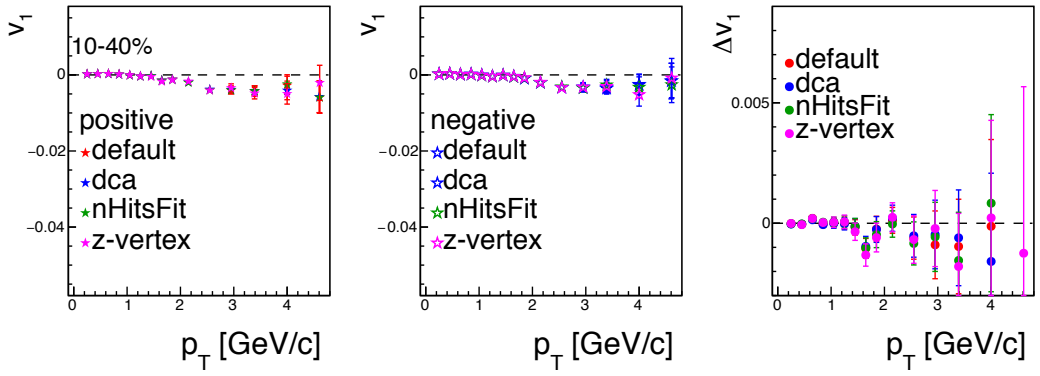

Fig. 34: v_1^{even} and Δv_1 as a function of p_T in 10-40% centrality in Au+Au collisions for different event/track seclection cuts

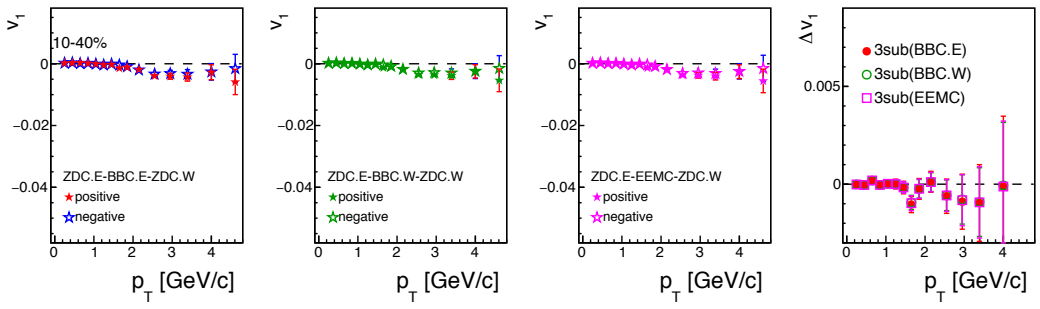

Fig. 35: v_1^{even} and Δv_1 as a function of p_T in 10-40% centrality in Au+Au collisions for different 3 sub combinations in the estmate of the event plane resolution

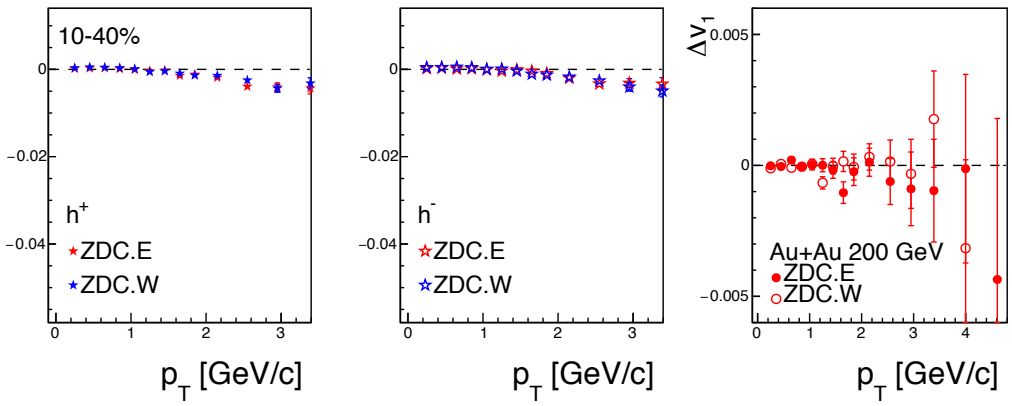

Fig. 36: v_1^{even} and Δv_1 as a function of p_T in 10-40% centrality in Au+Au collisions, measured with respect to ZDC-East and ZDC-West

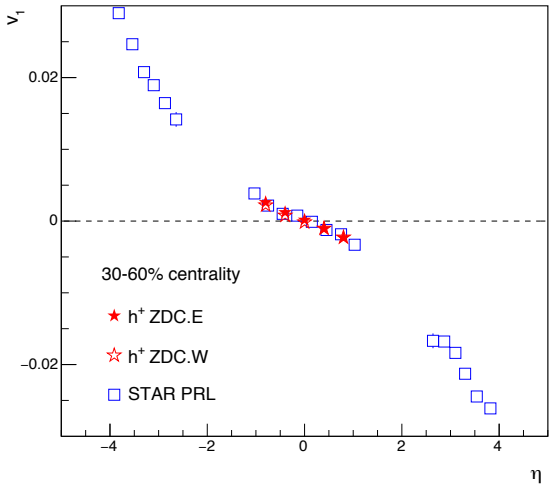

Fig. 37: v_1 of positive particles as a function of η in 30-60% centrality comparing with the STAR published result [8]

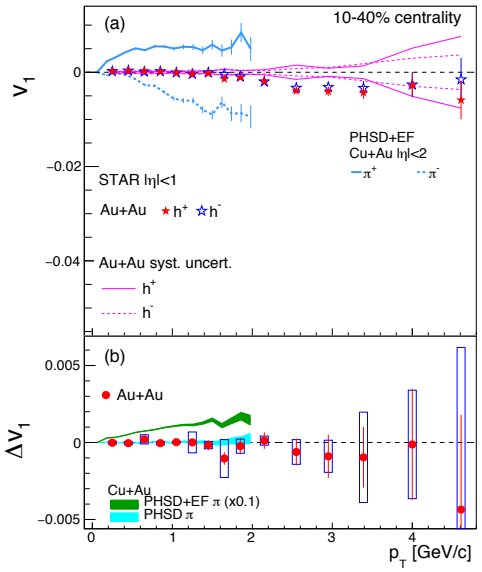

Fig. 38: v_1^{even} and Δv_1 as a function of p_T in 10-40% centrality in Au+Au collisions

C Effect from p and $\bar{p}$ in Δv_1

The STAR experiment published a paper on $v_1(y)$ of (anti)protons and charged pions from 200 GeV down to 7.7 GeV in Au+Au collisions [9]. The difference between protons and antiprotons except mid-rapidity (dv_1/dy difference) was observed even at 200 GeV (but not observed for pions). Since this difference could be a possible exlanation for η-dependence of Δv_1 observed in Cu+Au collisions, we investigated how much (anti)protons v_1 affects our results.

In order to simply check the effect, proton and antiproton samples were removed from charged particles in Cu+Au and Au+Au collisions. Therefore the following cuts were additinally applied to remove proton and antiproton candidates:

- $m^2 < 0.5$ if TOF information is available
- n$\sigma_p > 2$ if TOF information is not available

Figure 39 shows v_1 and Δv_1 as a function of *eta* for $0.15 < p_T < 2$ GeV/c and 10-40% centrality bin in Au+Au collisions. As observed for protons and antiprotons in Ref. [9], the similar charge difference can be seen. Since the p_T range of $1 < p_T < 2$

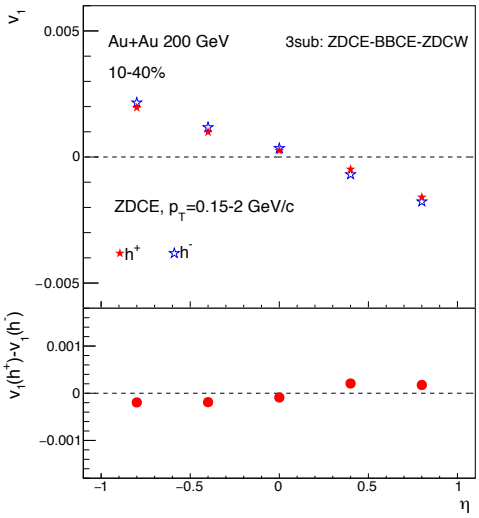

Fig. 39: $v_1(\eta)$ and $\Delta v_1(\eta)$ of charged particles for $0.15 < p_T < 2$ GeV/c and 10-40% centrality bin in Au+Au collisions

GeV/c was used in Cu+Au analysis, v_1 and Δv_1 in Au+Au collisions were measured using the same p_T range as shown in the left plot of Fig. 40. The difference becomes clear in that p_T range. The right plot of Fig. 40 shows v_1 and Δv_1 in Au+Au collisions after removing proton and antiproton candidates. The Δv_1 becomes consistent with zero.

When we compare $v_1(\eta)$ between Au+Au and Cu+Au collisions, it may not be a apple-to-apple comparison because the center-of-mass rapidity in Cu+Au would be shifted. Figure 41 shows $v_1(\eta)$ integrated over $p_T = 0.15-2$ GeV/c in Cu+Au collisions.

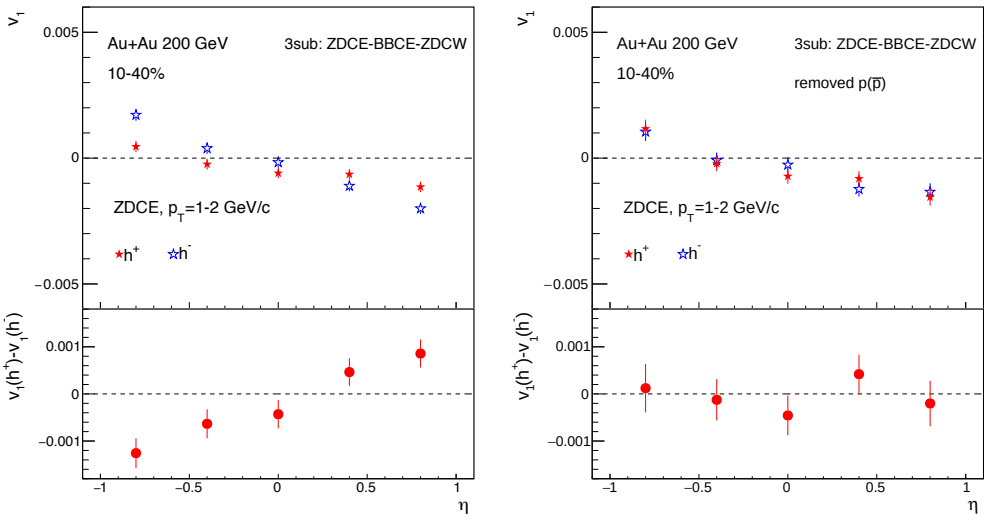

Fig. 40: $v_1(\eta)$ and $\Delta v_1(\eta)$ of charged particles for $1 < p_T < 2$ GeV/c and 10-40% centrality bin in Au+Au collisions. (Left) all charged particles (Right) charged particles after removing proton and antiproton candidates

The place where the v_1 crosses zero is around $\eta = 1$. If we compare $v_1(\eta = 1)$ in Cu+Au with $v_1(\eta = 0)$ in Au+Au, the sign of Δv_1 seems to be opposite. Also we performed the same test for Cu+Au as shown in Fig. 42. We can see still a finite positive Δv_1 even after the (anti)proton veto cuts. Therefore the Δv_1 we observed in Cu+Au collisions cannot be explained by the proton-antiproton difference observed in Au+Au collisions. Also, the Δv_1 in Cu+Au after the veto cuts seems to be less independent of η, although the statistical fluctuations are large.

Figure 43 shows $v_1(p_T)$ in Cu+Au collisions after the (anti)proton veto cuts. The similar pT dependence to the result without the veto cuts can be still seen.

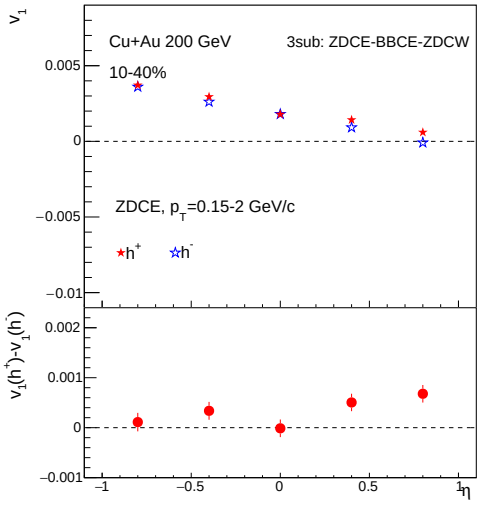

Fig. 41: $v_1(\eta)$ and $\Delta v_1(\eta)$ of charged particles for $0.15 < p_T < 2$ GeV/c and 10-40% centrality bin in Cu+Au collisions.

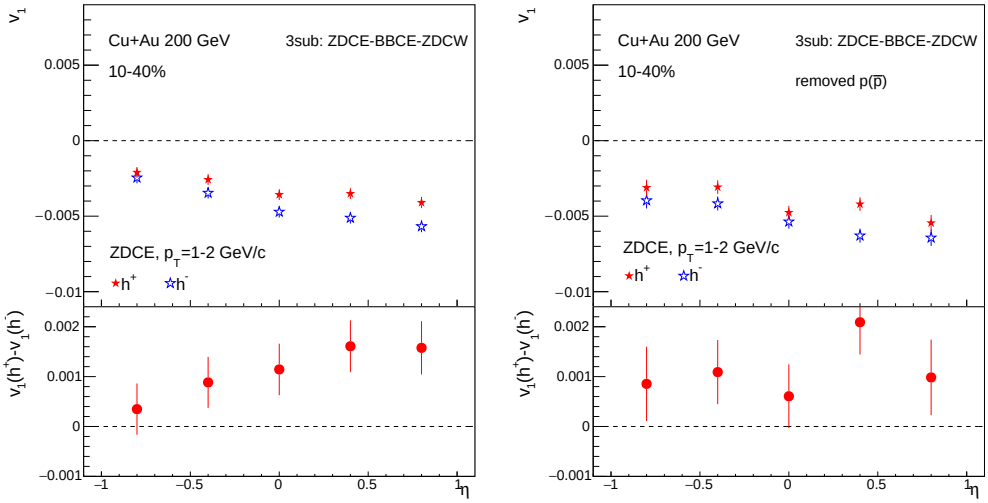

Fig. 42: $v_1(\eta)$ and $\Delta v_1(\eta)$ of charged particles for $1 < p_T < 2$ GeV/c and 10-40% centrality bin in Cu+Au collisions. (Left) all charged particles (Right) charged particles after removing proton and antiproton candidates

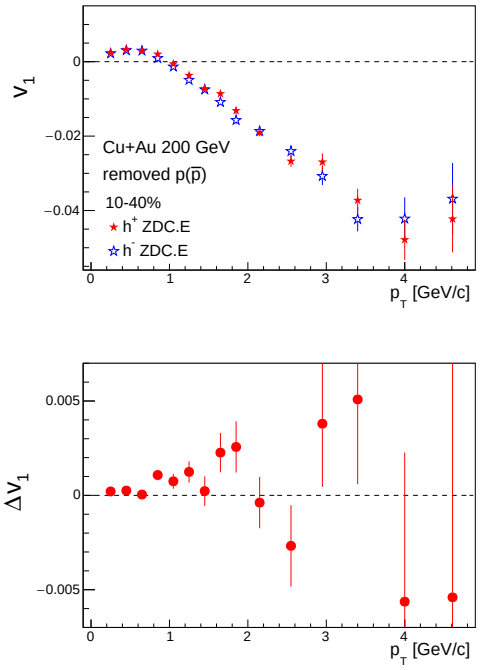

Fig. 43: $v_1(p_T)$ and $\Delta v_1(p_T)$ of charged particles in 10-40% centrality bin in Cu+Au collisions after removing proton and antiproton candidates.

References

[1] Y. Hirono, M. Hongo, and T. Hirano, Phys. Rev. C **90**, 021903 (2014)

[2] V. Voronyuk, V. D. Toneev, S. A. Voloshin, and W. Cassing, Phys. Rev. C **90**, 064903 (2014)

[3] J. Barrette *et al.* (E877 Collaboration), Phys. Rev. C **56**, 3254 (1997)

[4] J. Barrette *et al.* (E877 Collaboration), Phys. Rev. C **55**, 1420 (1997)

[5] A. M. Poskazer and S. A. Voloshin, Phys. Rev. C **58**, 1671 (1998)

[6] J. Adams *et al.* (STAR Collaboration), Phys. Rev. C **73**, 034903 (2006)

[7] A. Adare *et al.* (PHENIX Collaboration), arXiv:1509.07784 (2015)

[8] B. I. Abelev *et a;.* (STAR Collaboration), Phys. Rev. Lett **101**, 252301 (2008)

[9] L. Adamczyk *et al.* (STAR Collaboration), Phys. Rev. Lett **112**, 162301 (2014)